Molecules and Cells

Mitochondrial Ca^{2+} Uptake Relieves Palmitate-Induced Cytosolic Ca^{2+} Overload in MIN6 Cells

Luong Dai Ly[1,2], Dat Da Ly[1,2], Nhung Thi Nguyen[1,2], Ji-Hee Kim[2], Heesuk Yoo[3], Jongkyeong Chung[3], Myung-Shik Lee[4,5], Seung-Kuy Cha[1,2], and Kyu-Sang Park[1,2,*]

[1]Department of Physiology, [2]Mitohormesis Research Center, Yonsei University Wonju College of Medicine, Wonju 26426, Korea, [3]National Creative Research Initiatives Center for Energy Homeostasis Regulation, Institute of Molecular Biology and Genetics, Seoul National University, Seoul 08826, Korea, [4]Severance Biomedical Science Institute, [5]Department of Internal Medicine, Yonsei University College of Medicine, Seoul 03722, Korea
*Correspondence: qsang@yonsei.ac.kr
https://doi.org/10.14348/molcells.2019.0223
www.molcells.org

Saturated fatty acids contribute to β-cell dysfunction in the onset of type 2 diabetes mellitus. Cellular responses to lipotoxicity include oxidative stress, endoplasmic reticulum (ER) stress, and blockage of autophagy. Palmitate induces ER Ca^{2+} depletion followed by notable store-operated Ca^{2+} entry. Subsequent elevation of cytosolic Ca^{2+} can activate undesirable signaling pathways culminating in cell death. Mitochondrial Ca^{2+} uniporter (MCU) is the major route for Ca^{2+} uptake into the matrix and couples metabolism with insulin secretion. However, it has been unclear whether mitochondrial Ca^{2+} uptake plays a protective role or contributes to lipotoxicity. Here, we observed palmitate upregulated MCU protein expression in a mouse clonal β-cell, MIN6, under normal glucose, but not high glucose medium. Palmitate elevated baseline cytosolic Ca^{2+} concentration ($[Ca^{2+}]_i$) and reduced depolarization-triggered Ca^{2+} influx likely due to the inactivation of voltage-gated Ca^{2+} channels (VGCCs). Targeted reduction of MCU expression using RNA interference abolished mitochondrial superoxide production but exacerbated palmitate-induced $[Ca^{2+}]_i$ overload. Consequently, MCU knockdown aggravated blockage of autophagic degradation. In contrast, co-treatment with verapamil, a VGCC inhibitor, prevented palmitate-induced basal $[Ca^{2+}]_i$ elevation and defective $[Ca^{2+}]_i$ transients. Extracellular Ca^{2+} chelation as well as VGCC inhibitors effectively rescued autophagy defects and cytotoxicity. These observations suggest enhanced mitochondrial Ca^{2+} uptake via MCU upregulation is a mechanism by which pancreatic β-cells are able to alleviate cytosolic Ca^{2+} overload and its detrimental consequences.

Keywords: cytosolic Ca^{2+} overload, lipotoxicity, mitochondrial Ca^{2+} uniporter, oxidative stress, pancreatic β-cell

INTRODUCTION

The common features of type 2 diabetes mellitus (T2DM) include insulin resistance and pancreatic β-cell deterioration. The latter determines the onset of diabetes (Rorsman and Ashcroft, 2018). A number of studies show excessive free fatty acids (FFAs) contribute to β-cell dysfunction and cell death. Palmitate, stearate, and oleate are the major FFAs in human plasma (Hagenfeldt et al., 1972). When isolated human islets are exposed to high palmitate and high glucose, β-cells show endoplasmic reticulum (ER) dilation, swollen mitochondria, several enlarged autophagic vacuoles, and distorted nuclei (Martino et al., 2012). These morphologic changes result from lipotoxic pathways in which Ca^{2+} and reactive oxygen species (ROS) play key roles. Consistent with these mecha-

Received 27 September, 2019; revised 20 November, 2019; accepted 3 December, 2019; published online 13 January, 2020

eISSN: 0219-1032

nistic findings, the Paris Prospective Study reports increased plasma FFA concentration is one of independent risk factors of T2DM in subjects with a history of impaired glucose tolerance (Charles et al., 1997). Higher fasting FFA concentrations are associated with decreased insulin secretion after an oral glucose load in both children and adults (Salgin et al., 2012).

Palmitate is known to induce oxidative stress via effects on multiple metabolic pathways. These include increased mitochondrial FFA oxidation, ceramide-disrupted electron transport through complex I and III, misfolded protein-induced ROS generation via ER oxidoreductin 1α (ERO-1α) and protein disulfide isomerase (PDI), and cytosolic diacylglycerol-protein kinase C (PKC)-NADPH oxidase pathway (Ly et al., 2017; Oh et al., 2018). Oxidative stress is associated with ER Ca^{2+} release and store depletion (Eletto et al., 2014). Since protein folding machinery requires high luminal Ca^{2+}, ER Ca^{2+} depletion accumulates misfolded proteins, which then trigger ER stress responses (Back and Kaufman, 2012). Several studies emphasize ER Ca^{2+} loss and ER stress as causative factors in β-cell death (Cnop et al., 2010; Cunha et al., 2008; Karaskov et al., 2006; Lee et al., 2010). However, fewer studies look into palmitate-elicited Ca^{2+} dyshomeostasis in cytosol and other organelles, e.g., mitochondria and lysosomes. Uncontrolled elevation of cytoplasmic Ca^{2+} concentration ($[Ca^{2+}]_i$) may trigger many undesirable signaling pathways, including PKC, Ca^{2+}/calmodulin-dependent protein kinase IV, c-Jun N-terminal kinase, and mitogen-activated protein kinase, which are followed by activation of transcription factors such as ATF2, CEBP/δ, CREB, Egr-1, and CHOP (da Cunha et al., 2015). Cytosolic Ca^{2+} overload also activates calpains, caspases, proteases, phosphatases, and endonucleases, which then trigger nitrosative and oxidative stress, lipid peroxidation, and mitochondrial dysfunction resulting in apoptosis (Carafoli, 2002; Szydlowska and Tymianski, 2010).

Increased $[Ca^{2+}]_i$ can be sequestered and dispersed by active mitochondria through mitochondrial Ca^{2+} uniporter (MCU) (De Stefani et al., 2015). MCU transports Ca^{2+} into the mitochondrial matrix driven by dissipation of the electrical gradient across the inner mitochondrial membrane and this accelerates mitochondrial metabolic flux and ATP synthesis. In insulin-secreting cells, MCU-mediated Ca^{2+} uptake plays a crucial role in coupling metabolism and insulin secretion (Quan et al., 2015; Tarasov et al., 2012). In mitochondria-associated ER membrane, MCU transports released Ca^{2+} from the ER to the mitochondrial matrix (Arruda and Hotamisligil, 2015). Oxidative stress augments this Ca^{2+} transport and leads to excessive matrix Ca^{2+} accumulation and cytotoxicity (Choi et al., 2017). Therefore, mitochondrial Ca^{2+} uptake has a double-edged consequences; the beneficial effect from sequestrating and relieving $[Ca^{2+}]_i$ overload and the detrimental action of matrix Ca^{2+} burden resulting in permeability transition pore opening and cytochrome c release. This is an interesting point worth investigating in the pathogenesis of β-cell lipotoxicity.

This study clarifies the role of mitochondrial Ca^{2+} uptake via MCU in insulin-secreting cells experiencing lipotoxicity. Targeted reduction of MCU expression decreased mitochondrial ROS generation by palmitate but exacerbated both cytosolic Ca^{2+} overload and defective autophagic degradation. Surprisingly, we found palmitate upregulated MCU expression and thus enabled increased mitochondrial Ca^{2+} sequestration. This compensatory mechanism disappeared under high glucose condition. Attenuation of $[Ca^{2+}]_i$ overload by inhibiting Ca^{2+} influx protected palmitate-treated cells from autophagic blockage and cytotoxicity. These results suggest a novel compensatory mechanism in β-cells that protects against lipotoxicity and that is mediated by MCU maintenance of cytosolic Ca^{2+} homeostasis.

MATERIALS AND METHODS

Reagents

All chemicals were purchased from Sigma-Aldrich (USA), unless otherwise stated. Krebs-Ringer bicarbonate buffer (KRBB) solution contains (mM): 5.5 glucose, 0.5 $MgSO_4$, 3.6 KCl, 0.5 NaH_2PO_4, 2 $NaHCO_3$, 140 NaCl, 1.5 $CaCl_2$, 10 HEPES, and pH 7.4 titrated with NaOH. Palmitate (#P9767; Sigma-Aldrich) was conjugated with bovine serum albumin (BSA) (#A6003; Sigma-Aldrich) in a molar ratio of 5.5:1 as described in (Xu et al., 2015).

Cell culture

Mouse insulinoma MIN6 cells (RRID:CVCL_0431) were grown in 5.5 mM glucose Dulbecco's modified Eagle's medium (DMEM) (#11885-084; Thermo Fisher Scientific, USA) supplemented with 10% fetal bovine serum (FBS) (#16000-044; Thermo Fisher Scientific), 100 IU/ml penicillin, 100 μg/ml streptomycin and 50 μM β-mercaptoethanol at 37°C with 5% CO_2. Before experiments, cells were seeded into corresponding plates and incubated overnight. Culture medium was then exchanged for either 5.5, 11, or 25 mM glucose DMEM with 1% FBS followed by the addition of palmitate or BSA. Experiments were performed with cells passaged 26-30 times.

Plasmid transfection

As a ER luminal Ca^{2+} fluorescent reporter, pCAG G-CEPIA1er was a gift from Franck Polleux (Addgene plasmid #105012; http://n2t.net/addgene:105012; RRID:Addgene_105012). Tandem fluorescent LC3 reporter, ptfLC3 was a gift from Tamotsu Yoshimori (Addgene plasmid #21074; http://n2t.net/addgene:21074; RRID:Addgene_21074). In the acidic environment of lysosomes, GFP is degraded but mRFP is not. Yellow and red LC3 puncta then represent autophagosomes and autophagolysosomes, respectively (Kimura et al., 2007). Approximately 6-8 h after cell seeding at 70-90% confluency, cells were transiently transfected with the plasmid using X-tremeGENE HP DNA Transfection Reagent (#6366236001; Roche, Germany) and Opti-MEM I Reduced Serum Medium (#31985-062; Thermo Fisher Scientific) as diluent according to the manufacturer's protocol.

Confocal microscopy

Cells transfected with ptfLC3 were treated with palmitate or BSA followed by fixation with 4% paraformaldehyde for 15 min at room temperature in the dark. Images were captured using a confocal microscope (LSM 800; Zeiss, Germany) and its software (ZEN 2.3). Yellow and red puncta were quan-

tified using ImageJ software (National Institutes of Health [NIH]; https://imagej.nih.gov/ij/) and red and green puncta were colocalized programmatically with a macro (https://imagejdocu.tudor.lu/plugin/analysis/colocalization_analysis_macro_for_red_and_green_puncta/start) (Satir and Pamplie-ga, 2016).

Small interfering RNA (siRNA) transfection

Mouse MCU (siGENOME; #062849-01) and negative control (#SN-1002) siRNAs were purchased from Dharmacon (USA) and Bioneer (Korea), respectively. Cells were seeded on to a 6-well plate 24 h before siRNA transfection. Before the transfection, cells were washed twice with PBS and maintained in DMEM. Transfection was conducted using OptiMEM and Dharmafect 1 transfection reagent (#T-2001-03; Dharmacon) following the manufacturer's guideline. Twenty-four hours after transfection, OptiMEM was replaced by complete medium. Cells were maintained 72 h before treatment with palmitate.

Western blot analysis

Cells were seeded on to a 6-well plate followed by treatment of palmitate with or without drugs as indicated. Cells were washed three times with cold PBS, lysed using cold RIPA buffer (#89900; Thermo Fisher Scientific) supplemented with protease and phosphatase inhibitors (#5892791001 and #4906837001, respectively; Roche), and centrifuged (17,000 rpm, 30 min). Supernatants were run on SDS-PAGE. Proteins were electroblotted on to polyvinylidene difluoride membranes (Merck Millipore, USA), blocked with either 5% BSA or 6% skim milk for 1 h at room temperature, and incubated with primary antibodies overnight at 4°C. The following primary antibodies were used: phospho-PERK (Thr980; #3179), total PERK (#3192), phospho-eIF2α (Ser51; #3597), total eIF2α (#5324), CHOP (#2895), cleaved caspase-3 (#9661), MCU (#14997), VDAC (#4866), LC3A/B (#4108), and p62 (#5114) from Cell Signaling Technology (USA); total OXPHOS antibody cocktail (#ab110413) and β-actin (#ab6276) from Abcam (UK); GAPDH (#sc-47724) from Santa Cruz Biotechnology (USA). All antibodies were applied diluted in buffer containing 0.1% Tris-buffered saline and Tween 20 (TBST) with 5% BSA. Membranes were washed with TBST four times (5 min/time), and then incubated with horseradish peroxidase-linked secondary antibody against rabbit or mouse IgG (#31460 or #31450, respectively; Thermo Fisher Scientific) supplemented with 6% skim milk for 1 h at room temperature. Membranes were washed again with TBST five times and then developed using ECL solution (Luminata Forte, #WBLUF0100; Millipore Corp., USA). Immunoreactive bands were visualized by Chemi Doc XRS+ imaging system and quantified using Image Lab 6.0 (Bio-Rad, USA).

MTT assay

MIN6 cells were plated at 5×10^4 cells/well in a 96-well plate. Cells pre-treated for 30 min with drugs were then co-incubated with palmitate or control BSA for 24 h. MTT solution was prepared by dissolving 3-[4,5-dimethylthiazol-2-yl]-2,5-diphenyl tetrazolium bromide (#M2128; Sigma-Aldrich) in fresh DMEM medium at 0.5 mg/ml. MTT assay was initiated by replacing culture medium with 100 μl of MTT solution. The plate was wrapped in foil and placed in an incubator for 2 h. After careful removal of medium to avoid cell detachment, 100 μl of DMSO was added to each well to dissolve formazan crystals. The plate was then gently swirled for 10 min and the absorbance value of each well was measured at 570 nm and 650 nm (reference) by Epoch Microplate Spectrophotometer (Bio-Tek, USA).

Apoptotic assay

The number of cytoplasmic mono- and oligo-nucleosome-associated histone-DNA complexes in cell lysates was measured by sandwich ELISA assay (Cell Death Detection ELISA Plus kit, #11774425001; Roche). MIN6 cells (5×10^4 cells/well) were seeded into 96-well plate. Cells were pre-treated with drug for 30 min then co-incubated with 500 μM palmitate or BSA for 24 h. The assay was performed by adding 200 μl of kit lysis buffer to each well and incubating for 30 min at room temperature. After centrifugation, 20 μl of supernatant was collected, and manufacturer instructions were followed. After a 5 min incubation with a peroxidase substrate, absorbance values were measured at 405 nm and 490 nm (reference) by Epoch Microplate Spectrophotometer.

Intracellular and ER Ca^{2+} measurement

MIN6 (3×10^4) cells suspended in 500 μl of complete medium were seeded on to 12 mm L-poly-lysine coated coverslips embedded in a 4-well plate then treated with palmitate (500 μM, 24 h) or BSA. To measure cytosolic Ca^{2+}, cells were incubated with 5 μM Fura-2 AM dissolved in KRBB for 1 h at room temperature, washed three times with KRBB, and perfused with free-Ca^{2+} KRB buffer in the presence of 200 μM sulfinpyrazone unless noted otherwise. The chamber was placed into the IX-73 inverted microscope platform (Olympus, Japan) with a camera attachment (Prime-BSI CMOS camera; Teledyne Photometrics, USA) and an illuminator (pe-340Fura; CoolLED, UK). The fluorophore was alternately excited at 340 and 380 nm while emission was recorded at 510 nm using MetaFluor 6.1 (Molecular Devices, USA). Background-subtracted 340/380 Fura-2 AM ratio reflecting $[Ca^{2+}]_i$ changes was calculated. At the end of each experiment, 10 μM ionomycin dissolved in 1.5 mM Ca^{2+} KRBB was added to induce a maximal ratio for comparison between control and palmitate-treated cells. For ER Ca^{2+} measurement, we transfected cells with G-CEPIA1er 48 h before the experiment. Fluorescence emission at 535 nm was recorded and analyzed following excitation with 488 nm.

ROS measurement

MIN6 (3×10^4) cells were plated on to 12 mm L-poly-lysine coated coverslips embedded in a 4-well plate before treatment with palmitate (500 μM, 24 h) or BSA. Cells were incubated either with 2.5 μM CM-H_2DCFDA (2′-7′ dichlorofluorescin diacetate) (#C6827; Thermo Fisher Scientific) or 5 μM mitoSOX (#M36008; Thermo Fisher Scientific) for 10 min at 37°C to detect intracellular ROS or mitochondrial superoxide production, respectively. Excitation/emission wavelengths for DCF and mitoSOX were 490/535 nm and 514/560 nm, respectively. Fluorescence intensity was quantified using the

IX81 inverted microscope (Olympus) with MetaMorph 6.1 (Molecular Devices).

Statistical analysis

Data were analyzed in GraphPad Prism 6.01 (GraphPad Software, USA) and presented as mean ± SD or SEM if available. Representative Ca^{2+} traces were the average of two or more Ca^{2+} recordings. Cell responses from at least three independent experiments were displayed in jitter plots in combination with bar graphs. Student's *t*-test or one- or two-way ANOVA with Bonferroni post-hoc test was used. *P* values less than 0.05 were considered statistically significant.

RESULTS

Palmitate elicited Ca^{2+} and ROS-related pathogenic changes and apoptosis in MIN6 cells

First, we established a cytotoxic dose profile for palmitate in a mouse clonal pancreatic β-cell line, MIN6. Palmitate decreased cell viability, measured by MTT assay, in a dose-dependent manner (Fig. 1A). Lipotoxic cell death was confirmed by increased apoptotic DNA fragments (Fig. 1B). Palmitate markedly elevated intracellular and mitochondrial ROS accumulation (Figs. 1C and 1D). In addition, palmitate incubation abrogated cyclopiazonic acid (CPA)-induced $[Ca^{2+}]_i$ response, which reflects ER Ca^{2+} content (Figs. 1E and 1F). To demonstrate the loss of Ca^{2+} stores in the ER, we measured intraluminal Ca^{2+} using a fluorescent reporter,

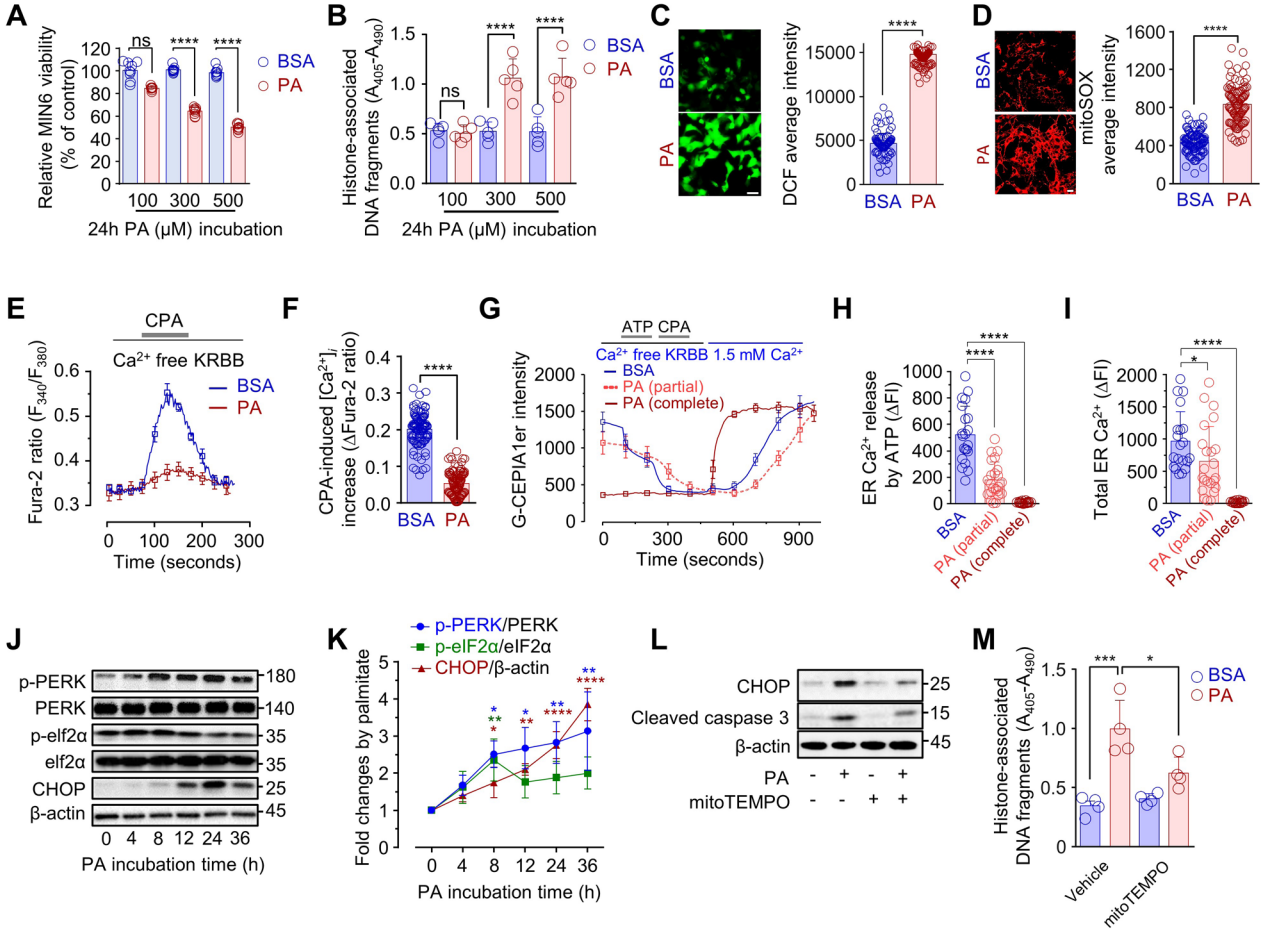

Fig. 1. Palmitate-induced oxidative stress and ER Ca^{2+} depletion resulted in ER stress and cell death. (A and B) Effects of different doses of palmitate (PA, 24 h) on MTT (A) and apoptotic DNA fragment (B) assays in MIN6 cells. (C and D) PA (500 μM)- or BSA-induced cytosolic ROS (C) and mitochondrial superoxide generation (D) measured by using DCF-DA and mitoSOX, respectively. Scale bars = 10 μm. (E and F) Cytosolic Ca^{2+} changes by CPA (20 μM), a SERCA inhibitor, in BSA- or PA-treated cells loaded with Fura-2 AM. (G-I) Changes in ER Ca^{2+} content by ATP (100 μM) or CPA in BSA- or PA-treated cells after transfection with CEPIA1er, a ER Ca^{2+} reporter. FI, fluorescence intensity. (J and K) Time kinetics of different ER stress markers during palmitate treatment. (L and M) Effect of mitochondrial ROS scavenger, mitoTEMPO (500 nM) on palmitate-induced CHOP and cleaved caspase 3 (L) and apoptotic DNA fragments (M). Data represent mean ± SD, except MTT assay data, which show mean ± SEM. Data were collected from more than three independent experiments and analyzed by either two-tailed Student's *t*-test or one-way ANOVA. ns, not significant; $*P < 0.05$; $**P < 0.01$; $***P < 0.001$; $****P < 0.0001$.

G-CEPIA1er. As expected, the majority of control BSA-treated cells showed the ATP-induced ER Ca^{2+} release mediated by IP_3. Subsequent application of CPA completely depleted ER Ca^{2+} stores. Interestingly, heterogeneous responses to ATP and CPA were observed among different cells with palmitate pre-incubation. One-third of palmitate-treated cells possessed an empty ER Ca^{2+} pool and agonist treatment did not release any further ER Ca^{2+}. The remaining two-thirds of cells had lower ER Ca^{2+} and showed a smaller Ca^{2+} response upon ATP stimulation compared to control BSA-treated cells (Figs. 1G-1I). Depletion of ER Ca^{2+} stores strongly activated store-operated Ca^{2+} entry, especially in cells with completely emptied ER Ca^{2+} pools (Fig. 1G).

Because ER Ca^{2+} disturbance has a detrimental effect on protein folding (Back and Kaufman, 2012), we investigated alterations in the PERK-mediated ER stress response during the course of palmitate incubation. Both PERK and eIF2α showed early activation, before 12 h of palmitate treatment. This was followed by an increase in CHOP expression (Figs. 1J and 1K). Upregulation of CHOP was concomitant with a decrease in phospho-eIF2α, which is a dephosphorylation target of CHOP (Novoa et al., 2001). To demonstrate the cross-talk between ER stress and oxidative stress, we tested ROS scavenger treatment to see if their reduction of oxidative stress also reduces the severity of palmitate induced ER stress. Indeed, mitoTEMPO, a mitochondria-targeted antioxidant, reduced CHOP protein levels and reduced the extent of caspase 3 activation (Fig. 1L). Furthermore, mitoTEMPO reduced DNA fragments indicative of lipotoxic cell death (Fig. 1M).

MCU knockdown did not improve palmitate-induced ER stress nor cell death

We have previously reported cellular oxidative stress triggers MCU-mediated Ca^{2+} uptake and ER Ca^{2+} release in myocytes

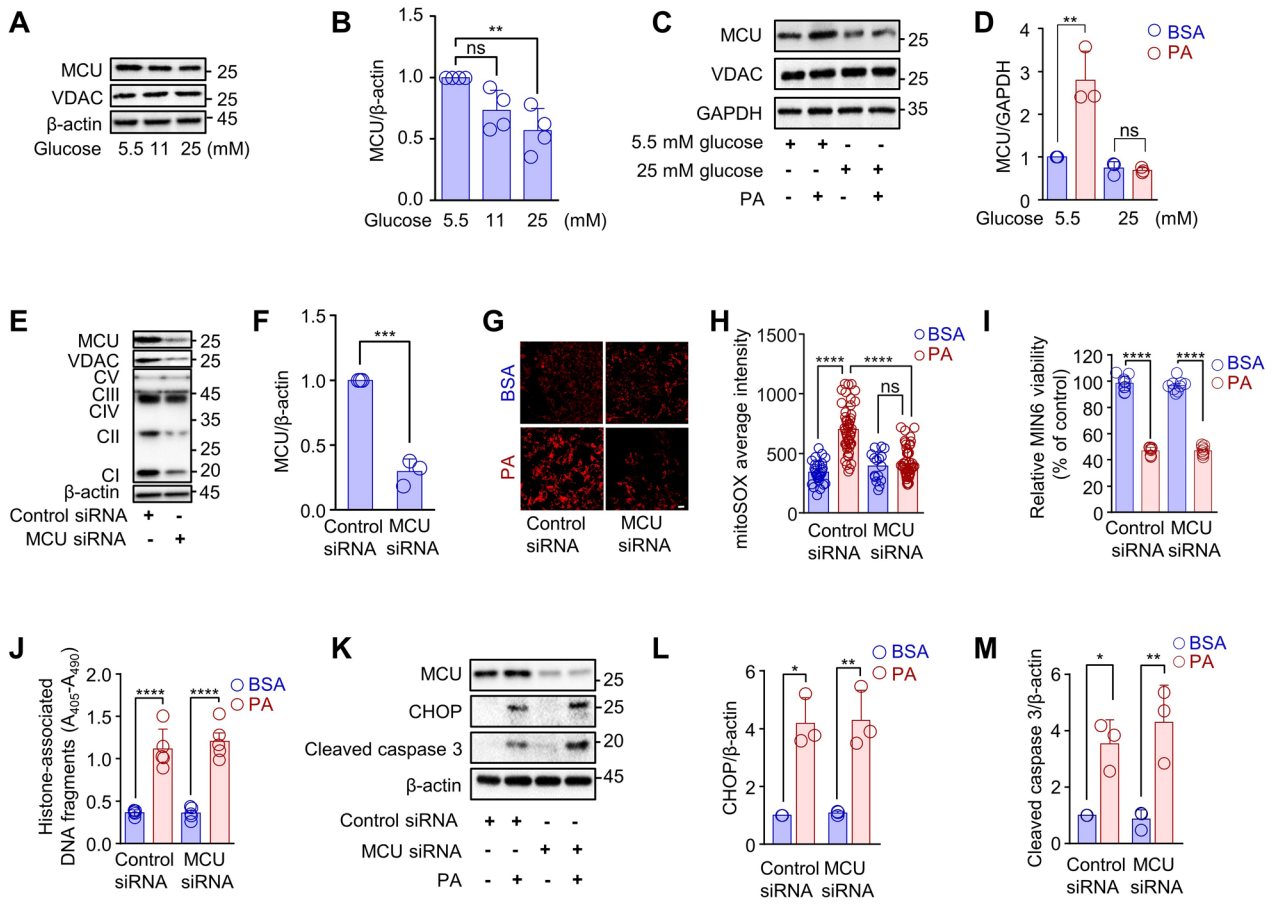

Fig. 2. MCU was upregulated by palmitate while MCU knockdown did not improve ER stress and cell death. (A and B) Representative immunoblotting and its quantitation of glucose effect on MCU expression in MIN6 cells. (C and D) Effect of glucose on palmitate (PA)-induced MCU upregulation. (E and F) Effect of siRNA-mediated MCU knockdown on the expression of VDAC and electron transport chain subunits. Complex I (CI): NDUFB8, complex II (CII): SDHB, complex III (CIII): UQCRC2, complex IV (CIV): MTCO1, and complex V (CV): ATP5A. (G and H) Effects of MCU knockdown on mitochondrial superoxide production by palmitate treatment. Scale bars = 10 μm. (I and J) Effects of MCU knockdown on palmitate-induced cytotoxicity determined by MTT (I) and apoptotic DNA fragment (J) assays. (K-M) Effects of MCU knockdown on CHOP and cleaved caspase-3 levels induced by palmitate incubation. Data represent mean ± SD, except MTT assay data, which show mean ± SEM. Data were collected from more than three independent experiments and analyzed by either two-tailed Student's *t*-test or one-way ANOVA. ns, not significant; $*P < 0.05$; $**P < 0.01$; $***P < 0.001$; $****P < 0.0001$.

of *Drosophila melanogaster* (Choi et al., 2017). To understand the role of mitochondrial Ca^{2+} uptake in glucolipotoxicity, we first checked MCU protein levels under high glucose or palmitate conditions. MCU expression was downregulated when cells in normal glucose (5.5 mM) medium were exposed to high glucose (25 mM) for 24 h (Figs. 2A and 2B). We then incubated MIN6 cells with palmitate (500 μM) for 24 h in either 5.5 or 25 mM glucose medium. Interestingly, palmitate significantly upregulated MCU protein expression under normal glucose medium but not under high glucose, while VDAC expression did not vary in either condition (Figs. 2C and 2D). To elucidate the pathophysiological role of upregulated MCU in palmitate-induced lipotoxicity, we reduced MCU expression by RNAi targeting, and reduction in protein level was confirmed by immunoblotting (Figs. 2E and 2F). MCU knockdown led to the downregulation of oxidative phosphorylation proteins, a phenomenon that was also previously demonstrated in a rat β-cell line, INS-1E (Quan et al., 2015). Silencing of MCU abolished mitochondrial superoxide generation in response to palmitate; this suggests a critical role for Ca^{2+} uptake in mitochondrial oxidative stress (Figs. 2G and 2H). However, MCU knockdown did not rescue cells from palmitate-induced cytotoxicity, as estimated by MTT and DNA fragments assays (Figs. 2I and 2J). Furthermore, MCU silencing did not attenuate palmitate-induced CHOP upregulation and caspase 3 cleavage (Figs. 2K-2M). These results suggest that mitochondrial Ca^{2+} uptake does not participate in palmitate-induced cytotoxicity despite its contribution

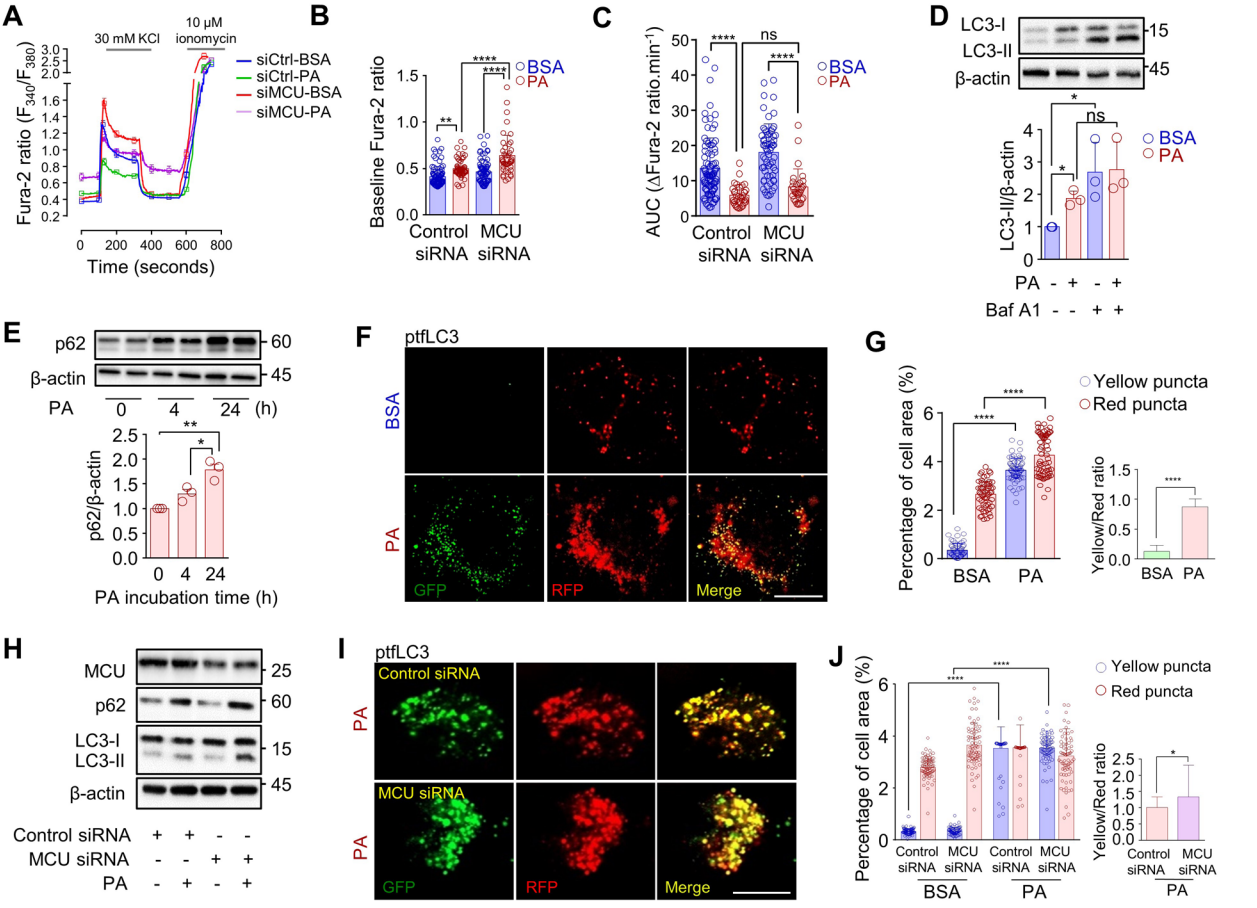

Fig. 3. Knockdown of MCU aggravated palmitate-induced cytosolic Ca^{2+} overload and defective autophagic degradation in MIN6 cells. (A-C) Representative traces of cytosolic Ca^{2+} concentration ($[Ca^{2+}]_i$) stimulated by KCl (30 mM) and ionomycin (10 μM) in MIN6 cells loaded with Fura-2 AM. Baseline $[Ca^{2+}]_i$ levels (B) and the area under the curve (AUC) of KCl-induced $[Ca^{2+}]_i$ changes (C) were compared between BSA- or palmitate (PA)-treated cells after transfection with control or MCU siRNA. (D) Immunoblotting and densitometry analysis of LC3 by palmitate with or without bafilomycin (Baf A1, 200 nM) added during last 2 h of palmitate incubation. (E) Time-dependent effect of palmitate on p62 expression. (F and G) Confocal images and quantitation of red/yellow LC3 puncta in BSA- or PA-treated cells after transfection with tandem fluorescent-tagged LC3 (ptfLC3) plasmid. Undigested autophagosomes are increased by palmitate determined by the ratio of yellow to red puncta (inset graph in Fig. 3G). (H) Effects of MCU knockdown on palmitate-induced alterations in p62 and LC3 proteins. (I and J) Effects of MCU knockdown on red/yellow LC3 puncta in BSA- or PA-treated cells after transfection of ptfLC3 plasmid. The ratio of yellow to red puncta is displayed in inset graph of Figure 3J. Data represent mean ± SD. Data were collected from more than three independent experiments and analyzed by either two-tailed Student's *t*-test or one-way ANOVA. ns, not significant; $*P < 0.05$; $**P < 0.01$; $****P < 0.0001$. Scale bars = 10 μm.

to ROS generation.

MCU silencing aggravated palmitate-induced cytosolic Ca^{2+} overload and defective autophagic degradation

In a pancreatic β-cell, glucose or other secretagogues increase $[Ca^{2+}]_i$ via voltage-gated Ca^{2+} channel (VGCC)-mediated influx or via Ca^{2+} release from the ER, which triggers insulin granule exocytosis (Gilon et al., 2014). The consequent removal of secretagogue relieves cytosolic Ca^{2+} load and returns the cytosol to the resting $[Ca^{2+}]_i$ level. We recorded changes in $[Ca^{2+}]_i$ using Fura-2 dye in response to high K^+-induced depolarization. Palmitate slightly elevated basal $[Ca^{2+}]_i$ levels but strongly attenuated the $[Ca^{2+}]_i$ response upon depolarization (Figs. 3A-3C). Suppression of mitochondrial Ca^{2+} uptake by MCU knockdown further elevated basal $[Ca^{2+}]_i$ in palmitate-treated cells, which could be caused by reduced mitochondrial Ca^{2+} sequestration (Figs. 3A and 3B).

Zummo et al. (2017) showed palmitate decreases autophagic flux in insulin-secreting cells by inhibiting the fusion of lysosomes and autophagosomes. Bafilomycin A1 is an inhibitor of lysosomal V-ATPase, which blocks luminal acidification and degradation of auophagolysosomes. We also observed that the LC3-II/β-actin ratio was elevated in palmitate-treated cells but not increased any further during bafilomycin A1 treatment, implying the formation of autophagolysosomes was suppressed by palmitate (Fig. 3D). Consistent with increases in LC3, p62 protein was increased during the treatment with palmitate (Fig. 3E). We further

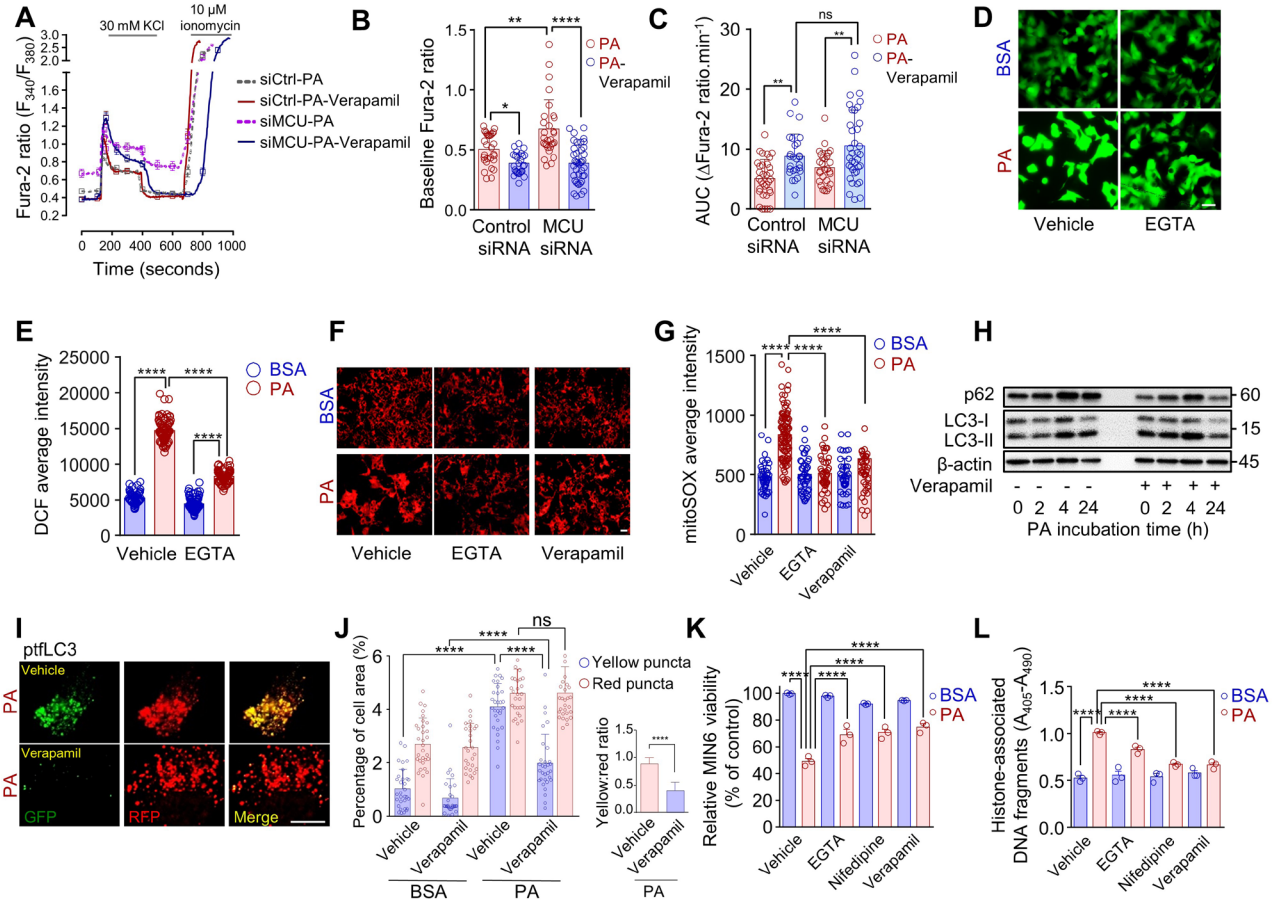

Fig. 4. Verapamil prevented palmitate-induced cytosolic Ca^{2+} overload, defective autophagic flux and lipotoxicity in MIN6 cells. (A) Representative traces of cytosolic Ca^{2+} concentration ($[Ca^{2+}]_i$) stimulated by KCl (30 mM) and ionomycin (10 μM) in MIN6 cells loaded with Fura-2 AM. Baseline $[Ca^{2+}]_i$ levels (B) and the area under the curve (AUC) of KCl-induced $[Ca^{2+}]_i$ changes (C) in the presence of palmitate were compared between vehicle- or verapamil (10 μM)-pretreated cells after transfection with control or MCU siRNA. (D-G) Effects of EGTA (0.4 mM)- or verapamil-pretreatment on palmitate-induced cytosolic ROS (D and E) and mitochondrial superoxide generation (F and G) measured by using DCF-DA and mitoSOX, respectively. (H) Immunoblotting of p62 and LC3 in palmitate-incubated cells with verapamil or vehicle pretreatment. (I and J) Confocal images and quantitation of red/yellow LC3 puncta in BSA- or PA-treated cells with vehicle- or verapamil pretreatment after transfection with ptfLC3 plasmid. The ratio of yellow to red puncta is displayed in inset graph of Fig. 4J). (K and L) Effects of EGTA, nifedipin (10 μM) or verapamil-pretreatment on palmitate-induced cytotoxicity determined by MTT (I) and apoptotic DNA fragment (J) assays. Data represent mean ± SD, except MTT assay data, which show mean ± SEM. Data were collected from more than three independent experiments and analyzed by either two-tailed Student's *t*-test or one-way ANOVA. ns, not significant; $*P < 0.05$; $**P < 0.01$; $****P < 0.0001$. Scale bars = 10 μm.

examined palmitate-elicited autophagic inhibition by using tandem fluorescent-tagged LC3 (ptfLC3) plasmid. Confocal microscopy revealed autophagosome and autophagolysosome puncta, and these are rendered in yellow and in red, respectively. Palmitate drastically increased the average cell area covered by yellow puncta while it modestly affected that of red puncta (Figs. 3F and 3G). As a result, the ratio of yellow to red puncta was significantly higher in palmitate-treated cells compared to BSA-treated cells (Fig. 3G, inset graph). We further estimated the effects of palmitate on autophagic flux in MCU-silenced and control cells. Immunoblots revealed that MCU ablation did not rescue p62 accumulation during lipotoxicity (Fig. 3H). Consistently, the extent of yellow puncta and the ratio of yellow to red puncta in palmitate-treated cell were not reduced but instead were augmented by MCU knockdown (Figs. 3I and 3J). Collectively, these data suggest that upregulation of MCU by palmitate mitigates cellular Ca^{2+} overload and alleviates autophagic block during β-cell lipotoxicity.

Attenuation of extracellular Ca^{2+} influx via VGCC alleviated Ca^{2+} overload and cytotoxicity by palmitate

One hypothesis suggests excessive Ca^{2+} influx from extracellular space through VGCCs could contribute to the palmitate-induced toxicity in insulin-secreting cells (Choi et al., 2007). Our data also indicate that inhibition of mitochondrial Ca^{2+} sequestration results in detrimental consequences of Ca^{2+} cytotoxicity by palmitate. Hence we next tested whether attenuating $[Ca^{2+}]_i$ overload could relieve the pathologic consequences of β-cell lipotoxicity. To reduce VGCC-mediated Ca^{2+} influx, we exposed cells to a Ca^{2+} chelator, EGTA, or to VGCC inhibitors verapamil or nifedipine. As expected, co-treatment with verapamil for 24 h abated basal $[Ca^{2+}]_i$ rise by palmitate (Figs. 4A and 4B). Preventive action of verapamil on $[Ca^{2+}]_i$ overload was more prominent in MCU silenced cells (Fig. 4B). In these experiments, we washed out verapamil thoroughly before measuring maximum voltage-gated Ca^{2+} flux, which we induced using high K^+. Pre-incubation with verapamil ameliorated the $[Ca^{2+}]_i$ response to depolarization both in control and MCU knockdown cells (Fig. 4C).

We observed that extracellular Ca^{2+} chelation with EGTA or VGCC inhibition with verapamil suppressed palmitate-induced cytosolic (Figs. 4D and 4E) and mitochondrial (Figs. 4F and 4G) ROS production. Moreover, verapamil reduced p62 accumulation during the entire period of palmitate treatment (Fig. 4H). Confocal imaging analysis with tandem fluorescent-tagged LC3 transfection revealed that verapamil pre-incubation decreased the number of yellow puncta and the ratio of yellow to red puncta in palmitate-treated cells (Figs. 4I and 4J). Finally, extracellular EGTA and VGCC inhibitors each rescued cell viability (Fig. 4K) and prevented apoptotic cell death (Fig. 4L). These results suggest that cytosolic Ca^{2+} burden due to extracellular Ca^{2+} influx is a critical pathogenic mechanism for autophagy defects and β-cell lipotoxicity. This Ca^{2+} overload by palmitate could be compensated by MCU-mediated Ca^{2+} sequestration.

DISCUSSION

In this study, we demonstrated ER Ca^{2+} release and store depletion by palmitate related to oxidative stress. ER Ca^{2+} depletion by palmitate leads to ER stress responses and cell death in mouse clonal pancreatic β-cells. These results are consistent with reports in other insulin-secreting cells (Gwiazda et al., 2009; Hara et al., 2014) and our previous observation in mouse podocytes (Xu et al., 2015). Several mechanisms have been suggested for palmitate-induced ER Ca^{2+} depletion. Binding to the fatty acid receptor coupled to Gq-protein (GPR40) can trigger IP_3-mediated ER Ca^{2+} release (Mancini and Poitout, 2013). Oxidative stress induced by palmitate may stimulate ER Ca^{2+} release channels directly (Li et al., 2009) or promote IP_3 generation via phospholipase Cγ (Weissmann et al., 2012). Released Ca^{2+} is taken up by sarco-/endoplasmic ER Ca^{2+} ATPase (SERCA) with ATP-consuming active processes. However, palmitate is known to decrease SERCA expression and activity, consequently reducing ER Ca^{2+} uptake and luminal Ca^{2+} content (Gustavo Vazquez-Jimenez et al., 2016; Hara et al., 2014; Zhang et al., 2014). Lowered Ca^{2+} in the ER deteriorates chaperone function. The accumulation of misfolded protein further aggravates oxidative stress via ERO-1α and PDI (Tu and Weissman, 2004). This positive feedback loop between oxidative stress and ER stress could activate pro-apoptotic downstream effectors in β-cell lipotoxicity.

We intended to scrutinize the alterations in ER Ca^{2+} content by using Ca^{2+} sensing fluorescent protein expressed exclusively in the ER lumen. This sensor successfully detected purinoceptor-mediated ER Ca^{2+} release, emptying of Ca^{2+} stores by ER Ca^{2+} ATPase inhibition, and Ca^{2+} refilling through store-operated Ca^{2+} entry (SOCE). We observed two patterns of ER Ca^{2+} disturbance by palmitate in insulin-secreting cells: (i) marked reduction but not depletion and (ii) complete loss of Ca^{2+} in the ER reservoir (Fig. 1G). Particularly, cells with the latter pattern have a steep $[Ca^{2+}]_i$ rise upon extracellular Ca^{2+} exposure; this implies full activation of SOCE. Previously, we observed a marked STIM1 oligomerization leading to persistent SOCE activation by palmitate in mouse podocytes (Xu et al., 2015). Furthermore, VGCC-mediated Ca^{2+} influx was also triggered by palmitate in insulin-secreting cells (Choi et al., 2007). The Ca^{2+} influx through SOCE and VGCC together with ER Ca^{2+} release might result in sustained elevated $[Ca^{2+}]_i$ in palmitate-treated cells (Gwiazda et al., 2009). Therefore, it is reasonable to infer that cytosolic Ca^{2+} overburden plays a pathogenic role in β-cell lipotoxicity.

In this study, we observed an increase in MCU expression induced by palmitate that has not been previously reported as far as we know. This upregulation could be a compensatory mechanism for cells to handle cytosolic Ca^{2+} overload in lipotoxicity. We directly measured the palmitate-induced elevation of basal $[Ca^{2+}]_i$ and noted that MCU silencing remarkably exacerbated this $[Ca^{2+}]_i$ burden (Figs. 3A and 3B). Mitochondrial Ca^{2+} uptake via MCU could sequester Ca^{2+} and relieve Ca^{2+} accumulation in peri-ER microdomains. Mitochondria are known to decrease movement and gather at high Ca^{2+} microdomains. Therefore, mitochondria can sequester Ca^{2+} from localized microdomains to avoid cytotoxicity (Yi et al.,

2004). It has been well known that high glucose exacerbates lipotoxicity in a synergistic manner in the progress of T2DM. Interestingly, our study showed that a high glucose environment decreased MCU expression and abated palmitate-mediated MCU upregulation. We speculate that high glucose eliminates the compensatory mechanism involving MCU and causes further serious consequences related to Ca^{2+} overload in β-cell lipotoxicity. This is the first proposal of a hypothesis for glucolipotoxicity.

We observed a significant reduction in mitochondrial superoxide generation by MCU knockdown, consistent with results from many other studies (Panahi et al., 2018; Ren et al., 2017; Tomar et al., 2019). This reduction could be attributed to the decrease in mitochondrial metabolism related to suppressed TCA cycle dehydrogenases and NADH shuttle system, which is sensitive to matrix Ca^{2+} (Denton, 2009). In addition, MCU knockdown correlates with downregulation of electron transport chain proteins (Fig. 2E), and this in turn could also decrease superoxide production. Unexpectedly, however, palmitate-induced ER stress and apoptosis were not prevented nor aggravated by MCU silencing. The ratio of yellow to red puncta from tandem fluorescent-tagged LC3 also became substantially higher in palmitate-treated MCU knockdown cells, indicating a possibly worsened defect in autophagolysosome formation (Park et al., 2014). Increased p62 accumulation upon MCU silencing supports the notion of deterioration in blocking autophagy. It is conceivable the benefits of attenuating mitochondrial Ca^{2+} uptake were offset by the negative consequences of impaired cytosolic Ca^{2+} clearance. Notably, all these pathologic alterations in palmitate-treated cells were rescued by agents that reduce Ca^{2+} influx from extracellular compartments, e.g., EGTA or VGCC inhibitors such as verapamil and nifedipine (Fig. 4). Our findings are consistent with a previous report that cytosolic Ca^{2+} overload impedes the fusion between autophagosomes and lysosomes in HepG2 cells (Park and Lee, 2014).

In pancreatic β-cells, ATP-sensitive K^+ channel (K_{ATP})-dependent $[Ca^{2+}]_i$ increase via VGCC is an important signal for glucose-stimulated insulin secretion (Wollheim and Maechler, 2002). In this study, depolarization-induced $[Ca^{2+}]_i$ increase was blunted by palmitate in MIN6 cells (Fig. 3A), and cells in this state displayed impaired insulin secretion upon nutrient stimulation. It has been known that $[Ca^{2+}]_i$ increase via VGCCs can suppress itself due to Ca^{2+}-dependent inactivation (Haack and Rosenberg, 1994). We infer that elevated $[Ca^{2+}]_i$ levels under lipotoxic conditions could inactivate VGCC directly and suppress K_{ATP}-dependent Ca^{2+} signal generation for insulin secretion. This may be the pathogenic mechanism responsible for insufficient insulin secretion and glucose intolerance in T2DM patients. Surprisingly, pretreatment of verapamil effectively recovered not only palmitate-induced $[Ca^{2+}]_i$ overload but also restored depolarization-triggered $[Ca^{2+}]_i$ response to normal. Preventive treatment with verapamil on β-cell lipotoxicity might result from beneficial actions of $[Ca^{2+}]_i$ regulation, making verapamil an effective preventive or therapeutic target for T2DM.

We demonstrated in this study that mitochondrial Ca^{2+} uptake via MCU upregulation could be an essential compensatory mechanism whereby cells alleviate cytosolic Ca^{2+} overload. Therefore, decreased mitochondrial Ca^{2+} sequestration due to mitochondrial dysfunction may aggravate palmitate-induced autophagy defects. Based on our observations, we suggest cytosolic Ca^{2+} overload in lipotoxicity could be relieved by i) suppressing Ca^{2+} influx, ii) accelerating mitochondrial Ca^{2+} clearance, or iii) enhancing Ca^{2+} recycling into the ER. Further investigation related to maintaining Ca^{2+} homeostasis may provide the best strategy against pancreatic β-cell failure and metabolic diseases.

Disclosure

The authors have no potential conflicts of interest to disclose.

ACKNOWLEDGMENTS

We thank the following authors: Daniel J. Shiwarski (University of Pittsburgh), Ruben K. Dagda (University of Nevada School of Medicine), and Charleen T. Chu (University of Pittsburgh) for sharing their ImageJ macro.

This work was supported by the Medical Research Center Program (2017R1A5A2015369) and National Research Foundation of Korea (NRF) Grant (2016R1A2B4014565) from Ministry of Science, ICT.

ORCID

Luong Dai Ly https://orcid.org/0000-0002-8824-8777
Dat Da Ly https://orcid.org/0000-0001-5092-5608
Nhung Thi Nguyen https://orcid.org/0000-0002-7057-0637
Ji-Hee Kim https://orcid.org/0000-0002-7980-4014
Heesuk Yoo https://orcid.org/0000-0002-0624-1118
Jongkyeong Chung https://orcid.org/0000-0001-5894-7537
Myung-Shik Lee https://orcid.org/0000-0003-3292-1720
Seung-Kuy Cha https://orcid.org/0000-0003-3201-7950
Kyu-Sang Park https://orcid.org/0000-0003-0322-9807

REFERENCES

Arruda, A.P. and Hotamisligil, G.S. (2015). Calcium homeostasis and organelle function in the pathogenesis of obesity and diabetes. Cell Metab. *22*, 381-397.

Back, S.H. and Kaufman, R.J. (2012). Endoplasmic reticulum stress and type 2 diabetes. Annu. Rev. Biochem. *81*, 767-793.

Carafoli, E. (2002). Calcium signaling: a tale for all seasons. Proc. Natl. Acad. Sci. U. S. A. *99*, 1115-1122.

Charles, M.A., Eschwege, E., Thibult, N., Claude, J.R., Warnet, J.M., Rosselin, G.E., Girard, J., and Balkau, B. (1997). The role of non-esterified fatty acids in the deterioration of glucose tolerance in Caucasian subjects: results of the Paris Prospective Study. Diabetologia *40*, 1101-1106.

Choi, S., Quan, X., Bang, S., Yoo, H., Kim, J., Park, J., Park, K.S., and Chung, J. (2017). Mitochondrial calcium uniporter in Drosophila transfers calcium between the endoplasmic reticulum and mitochondria in oxidative stress-induced cell death. J. Biol. Chem. *292*, 14473-14485.

Choi, S.E., Kim, H.E., Shin, H.C., Jang, H.J., Lee, K.W., Kim, Y., Kang, S.S., Chun, J., and Kang, Y. (2007). Involvement of Ca^{2+}-mediated apoptotic signals in palmitate-induced MIN6N8a beta cell death. Mol. Cell. Endocrinol. *272*, 50-62.

Cnop, M., Ladriere, L., Igoillo-Esteve, M., Moura, R.F., and Cunha, D.A. (2010). Causes and cures for endoplasmic reticulum stress in lipotoxic beta-cell dysfunction. Diabetes Obes. Metab. *12* Suppl 2, 76-82.

Cunha, D.A., Hekerman, P., Ladriere, L., Bazarra-Castro, A., Ortis, F., Wakeham, M.C., Moore, F., Rasschaert, J., Cardozo, A.K., Bellomo, E., et al.

(2008). Initiation and execution of lipotoxic ER stress in pancreatic beta-cells. J. Cell Sci. *121*, 2308-2318.

da Cunha, F.M., Torelli, N.Q., and Kowaltowski, A.J. (2015). Mitochondrial retrograde signaling: triggers, pathways, and outcomes. Oxid. Med. Cell. Longev. *2015*, 482582.

De Stefani, D., Patron, M., and Rizzuto, R. (2015). Structure and function of the mitochondrial calcium uniporter complex. Biochim. Biophys. Acta *1853*, 2006-2011.

Denton, R.M. (2009). Regulation of mitochondrial dehydrogenases by calcium ions. Biochim. Biophys. Acta *1787*, 1309-1316.

Eletto, D., Chevet, E., Argon, Y., and Appenzeller-Herzog, C. (2014). Redox controls UPR to control redox. J. Cell Sci. *127*, 3649-3658.

Gilon, P., Chae, H.Y., Rutter, G.A., and Ravier, M.A. (2014). Calcium signaling in pancreatic beta-cells in health and in Type 2 diabetes. Cell Calcium *56*, 340-361.

Gustavo Vazquez-Jimenez, J., Chavez-Reyes, J., Romero-Garcia, T., Zarain-Herzberg, A., Valdes-Flores, J., Manuel Galindo-Rosales, J., Rueda, A., Guerrero-Hernandez, A., and Olivares-Reyes, J.A. (2016). Palmitic acid but not palmitoleic acid induces insulin resistance in a human endothelial cell line by decreasing SERCA pump expression. Cell. Signal. *28*, 53-59.

Gwiazda, K.S., Yang, T.L., Lin, Y., and Johnson, J.D. (2009). Effects of palmitate on ER and cytosolic Ca^{2+} homeostasis in beta-cells. Am. J. Physiol. Endocrinol. Metab. *296*, E690-701.

Haack, J.A. and Rosenberg, R.L. (1994). Calcium-dependent inactivation of L-type calcium channels in planar lipid bilayers. Biophys. J. *66*, 1051-1060.

Hagenfeldt, L., Wahren, J., Pernow, B., and Raf, L. (1972). Uptake of individual free fatty acids by skeletal muscle and liver in man. J. Clin. Invest. *51*, 2324-2330.

Hara, T., Mahadevan, J., Kanekura, K., Hara, M., Lu, S., and Urano, F. (2014). Calcium efflux from the endoplasmic reticulum leads to beta-cell death. Endocrinology *155*, 758-768.

Karaskov, E., Scott, C., Zhang, L., Teodoro, T., Ravazzola, M., and Volchuk, A. (2006). Chronic palmitate but not oleate exposure induces endoplasmic reticulum stress, which may contribute to INS-1 pancreatic beta-cell apoptosis. Endocrinology *147*, 3398-3407.

Kimura, S., Noda, T., and Yoshimori, T. (2007). Dissection of the autophagosome maturation process by a novel reporter protein, tandem fluorescent-tagged LC3. Autophagy *3*, 452-460.

Lee, J.W., Kim, W.H., Yeo, J., and Jung, M.H. (2010). ER stress is implicated in mitochondrial dysfunction-induced apoptosis of pancreatic beta cells. Mol. Cells *30*, 545-549.

Li, G., Mongillo, M., Chin, K.T., Harding, H., Ron, D., Marks, A.R., and Tabas, I. (2009). Role of ERO1-alpha-mediated stimulation of inositol 1,4,5-triphosphate receptor activity in endoplasmic reticulum stress-induced apoptosis. J. Cell Biol. *186*, 783-792.

Ly, L.D., Xu, S., Choi, S.K., Ha, C.M., Thoudam, T., Cha, S.K., Wiederkehr, A., Wollheim, C.B., Lee, I.K., and Park, K.S. (2017). Oxidative stress and calcium dysregulation by palmitate in type 2 diabetes. Exp. Mol. Med. *49*, e291.

Mancini, A.D. and Poitout, V. (2013). The fatty acid receptor FFA1/GPR40 a decade later: how much do we know? Trends Endocrinol. Metab. *24*, 398-407.

Martino, L., Masini, M., Novelli, M., Beffy, P., Bugliani, M., Marselli, L., Masiello, P., Marchetti, P., and De Tata, V. (2012). Palmitate activates autophagy in INS-1E beta-cells and in isolated rat and human pancreatic islets. PLoS One *7*, e36188.

Novoa, I., Zeng, H., Harding, H.P., and Ron, D. (2001). Feedback inhibition of the unfolded protein response by GADD34-mediated dephosphorylation of eIF2alpha. J. Cell Biol. *153*, 1011-1022.

Oh, Y.S., Bae, G.D., Baek, D.J., Park, E.Y., and Jun, H.S. (2018). Fatty acid-induced lipotoxicity in pancreatic beta-cells during development of type 2 diabetes. Front. Endocrinol. (Lausanne) *9*, 384.

Panahi, G., Pasalar, P., Zare, M., Rizzuto, R., and Meshkani, R. (2018). MCU-knockdown attenuates high glucose-induced inflammation through regulating MAPKs/NF-kappaB pathways and ROS production in HepG2 cells. PLoS One *13*, e0196580.

Park, H.W. and Lee, J.H. (2014). Calcium channel blockers as potential therapeutics for obesity-associated autophagy defects and fatty liver pathologies. Autophagy *10*, 2385-2386.

Park, H.W., Park, H., Semple, I.A., Jang, I., Ro, S.H., Kim, M., Cazares, V.A., Stuenkel, E.L., Kim, J.J., Kim, J.S., et al. (2014). Pharmacological correction of obesity-induced autophagy arrest using calcium channel blockers. Nat. Commun. *5*, 4834.

Quan, X., Nguyen, T.T., Choi, S.K., Xu, S., Das, R., Cha, S.K., Kim, N., Han, J., Wiederkehr, A., Wollheim, C.B., et al. (2015). Essential role of mitochondrial Ca^{2+} uniporter in the generation of mitochondrial pH gradient and metabolism-secretion coupling in insulin-releasing cells. J. Biol. Chem. *290*, 4086-4096.

Ren, T., Zhang, H., Wang, J., Zhu, J., Jin, M., Wu, Y., Guo, X., Ji, L., Huang, Q., Zhang, H., et al. (2017). MCU-dependent mitochondrial Ca(2+) inhibits NAD(+)/SIRT3/SOD2 pathway to promote ROS production and metastasis of HCC cells. Oncogene *36*, 5897-5909.

Rorsman, P. and Ashcroft, F.M. (2018). Pancreatic β-cell electrical activity and insulin secretion: of mice and men. Physiol. Rev. *98*, 117-214.

Salgin, B., Ong, K.K., Thankamony, A., Emmett, P., Wareham, N.J., and Dunger, D.B. (2012). Higher fasting plasma free fatty acid levels are associated with lower insulin secretion in children and adults and a higher incidence of type 2 diabetes. J. Clin. Endocrinol. Metab. *97*, 3302-3309.

Satir, B.H. and Pampliega, O. (2016). Methods to study interactions between ciliogenesis and autophagy. Methods Mol. Biol. *1454*, 53-67.

Szydlowska, K. and Tymianski, M. (2010). Calcium, ischemia and excitotoxicity. Cell Calcium *47*, 122-129.

Tarasov, A.I., Semplici, F., Ravier, M.A., Bellomo, E.A., Pullen, T.J., Gilon, P., Sekler, I., Rizzuto, R., and Rutter, G.A. (2012). The mitochondrial Ca^{2+} uniporter MCU is essential for glucose-induced ATP increases in pancreatic beta-cells. PLoS One *7*, e39722.

Tomar, D., Jana, F., Dong, Z., Quinn, W.J., 3rd, Jadiya, P., Breves, S.L., Daw, C.C., Srikantan, S., Shanmughapriya, S., Nemani, N., et al. (2019). Blockade of MCU-mediated Ca^{2+} uptake perturbs lipid metabolism via PP4-dependent AMPK dephosphorylation. Cell Rep. *26*, 3709-3725.e7.

Tu, B.P. and Weissman, J.S. (2004). Oxidative protein folding in eukaryotes: mechanisms and consequences. J. Cell Biol. *164*, 341-346.

Weissmann, N., Sydykov, A., Kalwa, H., Storch, U., Fuchs, B., Mederos y Schnitzler, M., Brandes, R.P., Grimminger, F., Meissner, M., Freichel, M., et al. (2012). Activation of TRPC6 channels is essential for lung ischaemia-reperfusion induced oedema in mice. Nat. Commun. *3*, 649.

Wollheim, C.B. and Maechler, P. (2002). Beta-cell mitochondria and insulin secretion: messenger role of nucleotides and metabolites. Diabetes *51* Suppl 1, S37-S42.

Xu, S., Nam, S.M., Kim, J.H., Das, R., Choi, S.K., Nguyen, T.T., Quan, X., Choi, S.J., Chung, C.H., Lee, E.Y., et al. (2015). Palmitate induces ER calcium depletion and apoptosis in mouse podocytes subsequent to mitochondrial oxidative stress. Cell Death Dis. *6*, e1976.

Yi, M., Weaver, D., and Hajnoczky, G. (2004). Control of mitochondrial motility and distribution by the calcium signal: a homeostatic circuit. J. Cell Biol. *167*, 661-672.

Zhang, J., Li, Y., Jiang, S., Yu, H., and An, W. (2014). Enhanced endoplasmic reticulum SERCA activity by overexpression of hepatic stimulator substance gene prevents hepatic cells from ER stress-induced apoptosis. Am. J. Physiol. Cell Physiol. *306*, C279-C290.

Zummo, F.P., Cullen, K.S., Honkanen-Scott, M., Shaw, J.A.M., Lovat, P.E., and Arden, C. (2017). Glucagon-like peptide 1 protects pancreatic β-cells from death by increasing autophagic flux and restoring lysosomal function. Diabetes *66*, 1272-1285.